Investigation of energy transport in DIII-D High-β_P EAST-demonstration discharges with the TGLF turbulent and NEO neoclassical transport models

OPEN ACCESS
IOP Publishing | International Atomic Energy Agency
Nuclear Fusion
Nucl. Fusion **57** (2017) 036018 (11pp)
doi:10.1088/1741-4326/aa4ff8

Investigation of energy transport in DIII-D High-β_P EAST-demonstration discharges with the TGLF turbulent and NEO neoclassical transport models

C. Pan[1], G.M. Staebler[2], L.L. Lao[2], A.M. Garofalo[2], X. Gong[1], Q. Ren[1], J. McClenaghan[3], G. Li[1], S. Ding[1], J. Qian[1], B. Wan[1], G. S. Xu[1], W. Solomon[2], O. Meneghini[2] and S.P. Smith[2]

[1] Institute of Plasma Physics, Chinese Academy of Sciences, Hefei 230031, People's Republic of China
[2] General Atomics, PO Box 85608, San Diego, CA 92168-5608, USA
[3] Oak Ridge Associated Universities, Oak Ridge, TN 37831, USA

E-mail: ckpan@ipp.ac.cn

Received 30 August 2016, revised 8 November 2016
Accepted for publication 24 November 2016
Published 11 January 2017

Abstract

Energy transport analyses of the DIII-D high-β_P EAST-demonstration discharges have been performed using the TGYRO transport package with the TGLF turbulent and NEO neoclassical transport models under the OMFIT integrated modeling framework. Ion energy transport is shown to be dominated by neoclassical transport and ion temperature profiles predicted by TGYRO agree closely with the experimental measured profiles for these high-β_P discharges. Ion energy transport is largely insensitive to reductions in the $E \times B$ flow shear stabilization. The Shafranov shift is shown to play a role in the suppression of the ion turbulent energy transport below the neoclassical level. Electron turbulent energy transport is under-predicted by TGLF and a significant shortfall in the electron energy transport over the whole core plasma is found with TGLF predictions for these high-β_P discharges. TGYRO can successfully predict the experimental ion and electron temperature profiles by artificially increasing the saturated turbulence level for ETG driven modes used in TGLF.

Keywords: high-β_P, energy transport, EXB, Shafranov shif

(Some figures may appear in colour only in the online journal)

1. Introduction

A high fraction of bootstrap current, f_{BS}, the self-generated current due to the plasma density and temperature gradients [1–4], is desirable for steady-state tokamak operation, especially for future fusion reactor operation. It will minimize the need for external current drive. High poloidal beta β_P and high normalized toroidal beta β_N are the characteristics of the DIII-D high-β_P and high bootstrap current fraction discharges [5]. Here $\beta_P = \beta_T(B_{TA}/B_{PA})^2$ with $\beta_T = p_A/(B_{TA}^2/2\mu_0)$ is the dimensionless plasma pressure, and B_{TA} is the toroidal magnetic field at the plasma geometry center, B_{PA} is the averaged poloidal magnetic field for normalization, p_A is the volume average plasma pressure; and $\beta_N = \beta_T/(I_P/aB_T)$ with I_P is the total plasma current and a is the plasma minor radius. Recently the high-β_P experiments with EAST-similar operational conditions have been realized on the DIII-D tokamak by the joint DIII-D and EAST teams [6–10]. This research is to develop and test a possible scenario for the steady-state operation on the EAST tokamak. The superconducting EAST tokamak aims at the demonstration of long-pulse high performance plasma operation [11]. The DIII-D/EAST joint experiments

aim to develop on DIII-D a fully non-inductive operating scenario compatible with the EAST hardware constraints. The good confinement observed in these high-β_P discharges is investigated in this paper.

As is well known, the cross-field energy transport in the tokamak plasmas generally exceeds the neoclassical predictions. Understanding the underlying processes can increase our confidence in the extrapolation of present tokamak behaviors towards reactor regimes. It is commonly accepted that most of the transport in the tokamak plasmas is driven by plasma turbulence. The turbulent transport is mainly produced by micro-instabilities including, but not limited to, ion temperature gradient (ITG) driven modes, trapped electron modes (TEMs), and electron temperature gradient (ETG) driven modes.

Solving the fundamental gyrokinetic equations for the turbulent transport is computationally expensive to predict the profiles on a transport time scale. Reduced transport models of the turbulent transport, such as TGLF [12–15], have been developed and implemented in analysis and predictive codes. TGLF, which is calibrated to GYRO [16] non-linear simulation results and is widely used to analyze and predict the turbulent transport in the tokamak plasmas [17–23], is a quasi-linear transport model that uses a reduced gyro-fluid system of moments of the linear gyrokinetic equation to compute the spectrum of linear eigenmode instabilities. The linear eigenmodes and a model of the saturated turbulence fluctuation amplitude are combined to compute the fluxes of energy, particle and momentum.

The first-principle code NEO [24–26], provides an accurate numerical solution of the drift-kinetic equation and computes the neoclassical and classical collisional transport fluxes. NEO can calculate more accurate edge bootstrap current, which is important for the kinetic equilibrium reconstructions in the high-β_P and high collisionality tokamak plasmas [27].

TGLF + NEO has proven to be an accurate predictive theory-based transport model for the core of L-mode, H-mode inductive discharges, and DIII-D hybrid regimes [17–19, 28]. The high-β_P discharges push into plasma conditions that are quite different from the discharges where TGLF + NEO have been successful at predicting transport. It is important to test and validate the prediction ability of TGLF + NEO in the high-β_P experiments.

TGYRO [29, 30], which can utilize GYRO or TGLF for turbulent transport and NEO for neoclassical transport, is a transport manager that has been integrated into the OMFIT (one modeling framework for integrated tasks) framework [31, 32]. The TGLF turbulent and NEO neoclassical transport models will be used in the present analyses. TGYRO calculates the steady-state temperature profiles, which yield the total energy flux equal to the target flux given by the volume integrals of relevant energy source and sink terms.

The remaining part of this paper is organized as follows. In section 2, the overview of the high-β_P discharges to be analyzed will be presented. In section 3, the ion and electron energy transport will be analyzed in details. In section 4, the conclusions and discussions will be presented.

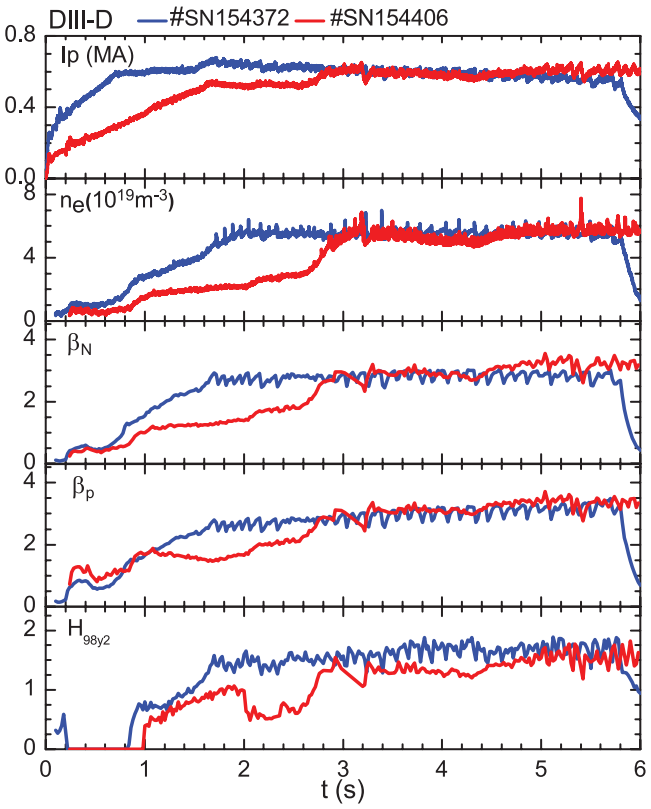

Figure 1. Overview of the DIII-D high-β_P discharges 154372 and 154406.

2. EAST-demonstration high-β_P discharges on DIII-D

Plasma production using a slow plasma current ramp-up rate consistent with the constraints of the superconducting coils on EAST was demonstrated on the DIII-D tokamak. The joint experiments on DIII-D exhibit excellent confinement, $H_{98y2} \sim 1.5$, with $\beta_N \sim 3$ and $\beta_P \sim 3$ [6–10]. High-β_P enables fully non-inductive discharges with the excellent confinement quality, desirable for the steady-state demonstration on the EAST tokamak. One of the important features of these high-β_P discharges is that a large radius ITB (internal transport barrier) is sustained.

Energy transport analyses have been performed for several discharges from the DIII-D high-β_P experiments and the results are similar. This paper will focus the discussions on the analysis of discharges 154372 and 154406 that exhibit excellent confinement with the lower NBI torque expected on EAST. An overview of these discharges is shown in figure 1. These discharges have good confinement, $H_{98y2} > 1.5$, with $\beta_N \sim 3$ and with a large radius ITB. The energy transport analyses will be performed for discharge 154372 at $t = 3.0$ s, 4.0 s and discharge 154406 at $t = 5.17$ s with the plasma current ~0.6 MA (0.597–0.613 MA), the vacuum toroidal magnetic field at the center of the vacuum vessel of −2.0 T, the line-averaged electron density, the safety factor on axis q_0 and q_{95} ranging from $4.81 - 5.35 \times 10^{19}\,\mathrm{m}^{-3}$, 2.7–3.96 and 10.4–12.3 respectively, which are listed in table 1. Kinetic equilibria at these time slices are reconstructed using the edge bootstrap

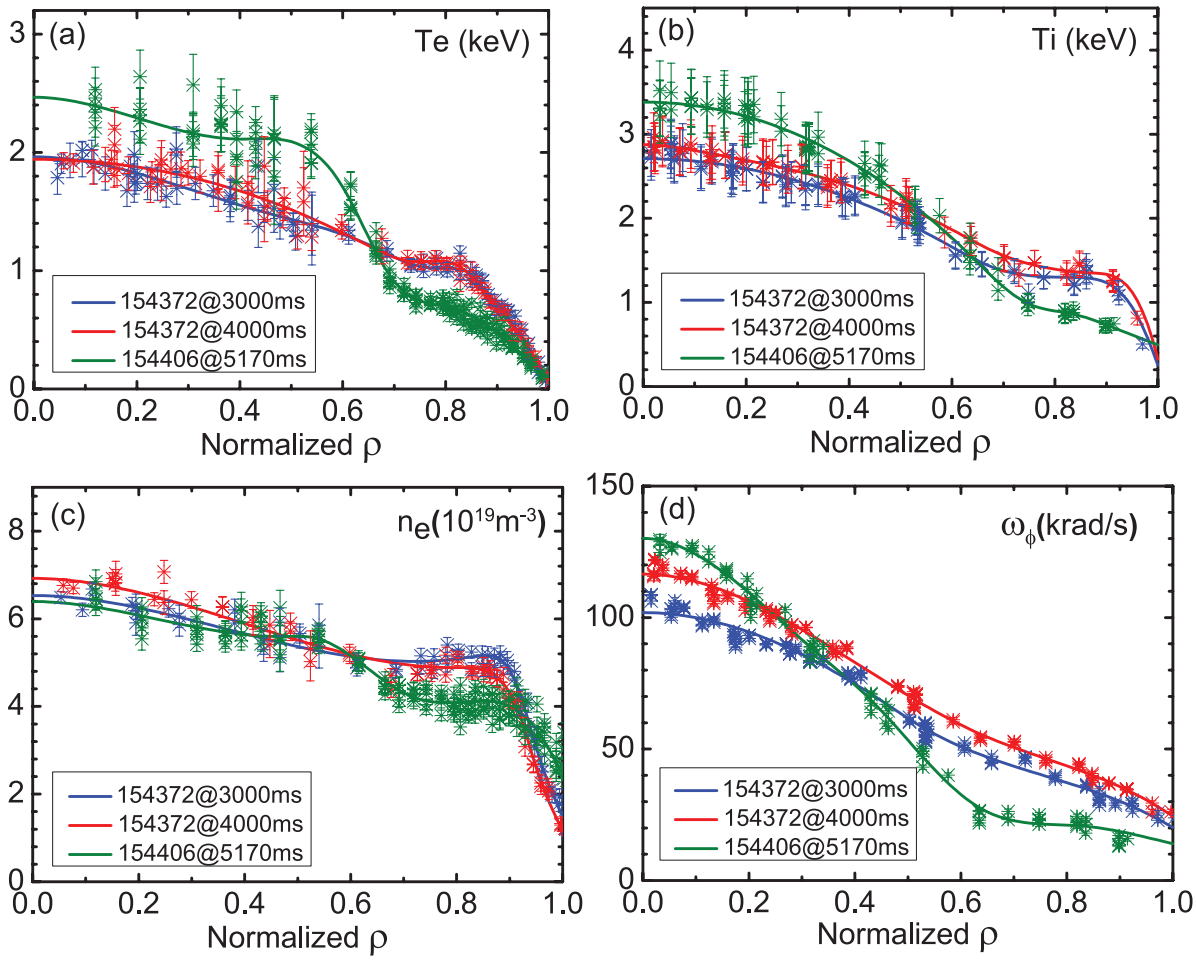

Figure 2. Profiles of (*a*) electron temperature, (*b*) ion temperature, (*c*) electron density, (*d*) toroidal rotation for the DIII-D high-β_P discharge 154372 at $t = 3.0$ s, 4.0 s and discharge 154406 at $t = 5.17$ s.

Table 1. Key parameters for discharge 154372 at $t = 3.0$ s, 4.0 s and discharge 154406 at $t = 5.17$ s: the plasma current I_P, the vacuum toroidal magnetic field at the center of the vacuum vessel B_{t0}, the line-averaged electron density $\overline{n}_e$, the safety factor on axis q_0, and q_{95}.

DIII-D plasma	I_P (MA)	B_{t0} (T)	$\overline{n}_e$ (10^{19} m^{-3})	q_0	q_{95}
154372@3.0 s	0.613	2.0	4.81	2.70	10.4
154372@4.0 s	0.597	2.0	4.89	3.28	11.0
154406@5.17 s	0.600	2.0	5.35	3.96	12.3

current calculated by NEO as a constraint. The plasma kinetic profiles for these time slices are shown in figure 2. There are high q_{95}(>10) and high bootstrap current fraction (>70%) as shown in figures 3 and 4 for these high-β_P discharges. The energy transport analysis results will be presented in the following section.

3. Energy transport analyses by TGYRO with TGLF + NEO

In this paper, we focus on the ion and electron energy transport and the steady-state ion and electron temperature profiles will be predicted by TGYRO with TGLF + NEO. The total calculated energy flux is composed of the turbulent energy flux calculated by the TGLF model and the neoclassical energy flux calculated by the NEO model. The predicted ion and electron temperature profiles are obtained by matching the total calculated energy flux with the target energy flux that is calculated with the experimental energy sources and sinks from the ONETWO transport code [33]. The energy sources and sinks include the auxiliary heating, the radiation loss and the energy exchange between the ions and the electrons which is computed self-consistently in TGYRO.

3.1. Ion neoclassical energy transport

Firstly, the ion energy transport is analyzed. The electron temperature profile and the other profiles (ion and electron density, toroidal rotation) are kept fixed and only the ion temperature profile is predicted by TGYRO with TGLF + NEO to distinguish the ion and electron channel energy transport. The boundary condition is imposed at $\rho = 0.8$. Figures 5(*a*)–(*c*) show the ion temperature profiles from the experimental data fit (blue lines) and the TGYRO predictions (red lines) for discharge 154372 at $t = 3.0$ s, 4.0 s and discharge 154406

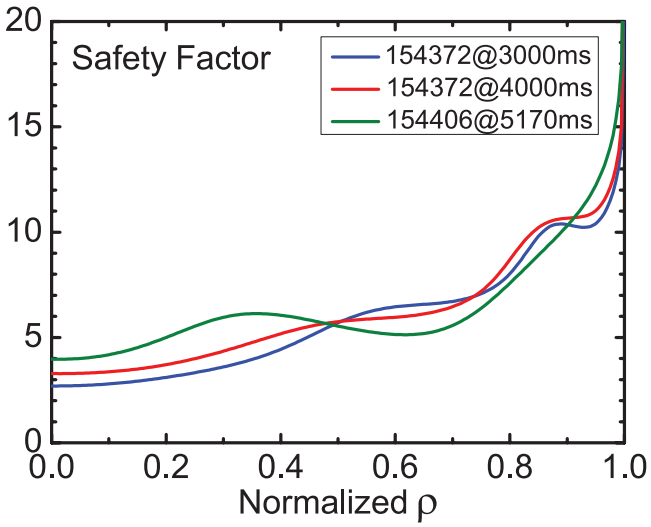

Figure 3. Safety factor profiles for the DIII-D high-β_P discharge 154372 at $t = 3.0$ s, 4.0 s and discharge 154406 at $t = 5.17$ s.

at $t = 5.17$ s respectively. The predicted ion temperature profiles agree very closely with the experimental measured ones well within the measurement error shown in figure 2(*b*). Figures 5(*d*)–(*f*) shows the ion neoclassical and turbulent energy fluxes calculated with TGLF and NEO respectively. The total calculated energy flux is also shown in figures 5(*d*)–(*f*). It is clear that the ion energy transport is dominated by the neoclassical energy transport. The ion turbulent energy transport is small and negligible inside $\rho \sim 0.63$. The ion energy transport is on the neoclassical level inside $\rho = 0.8$. The ion neoclassical transport is strongly related to the ion banana orbit width, which is proportional to the safety factor and the poloidal gyro-radius. The ion banana orbit is large due to the high safety factor q and high β_P in these high-β_P discharges. The large ion neoclassical energy transport will reduce the ion temperature gradient and it may play a role in the formation of ion-ITB by keeping the ion temperature gradient below the ITG threshold.

It is well known that $E \times B$ flow shear [34, 35] has a stabilizing effect on the low-k micro-instabilities, such as ITG and TEM modes. There are experiments with strong flow shear such that the ion energy transport is reduced to the neoclassical level [36]. This is the conventional definition of an ITB. It has been validated that the ITG is suppressed by the $E \times B$ flow shear within the ITB for these cases. To study the effect of $E \times B$ flow shear on the ion energy transport in the DIII-D high-β_P discharges, the predictions of the ion energy transport by TGYRO with the $E \times B$ turned off artificially are performed as shown in figure 6. The ion temperature profiles predicted by TGYRO without $E \times B$ as shown by the olive lines in figures 6(*a*)–(*c*) are similar to that predicted by TGYRO with $E \times B$ as shown by the red lines in figures 6(*a*)–(*c*). The ion energy transport is largely insensitive to the $E \times B$ flow shear in these high-β_P discharges. The ion turbulent energy transport in discharge 154372 at $t = 3.0$ s and $t = 4.0$ s increases with the $E \times B$ turned off as shown by the olive lines in figures 6(*d*) and (*e*), but it is still much smaller than the neoclassical energy flux as shown by the blue lines in figures 6(*d*) and (*e*). While

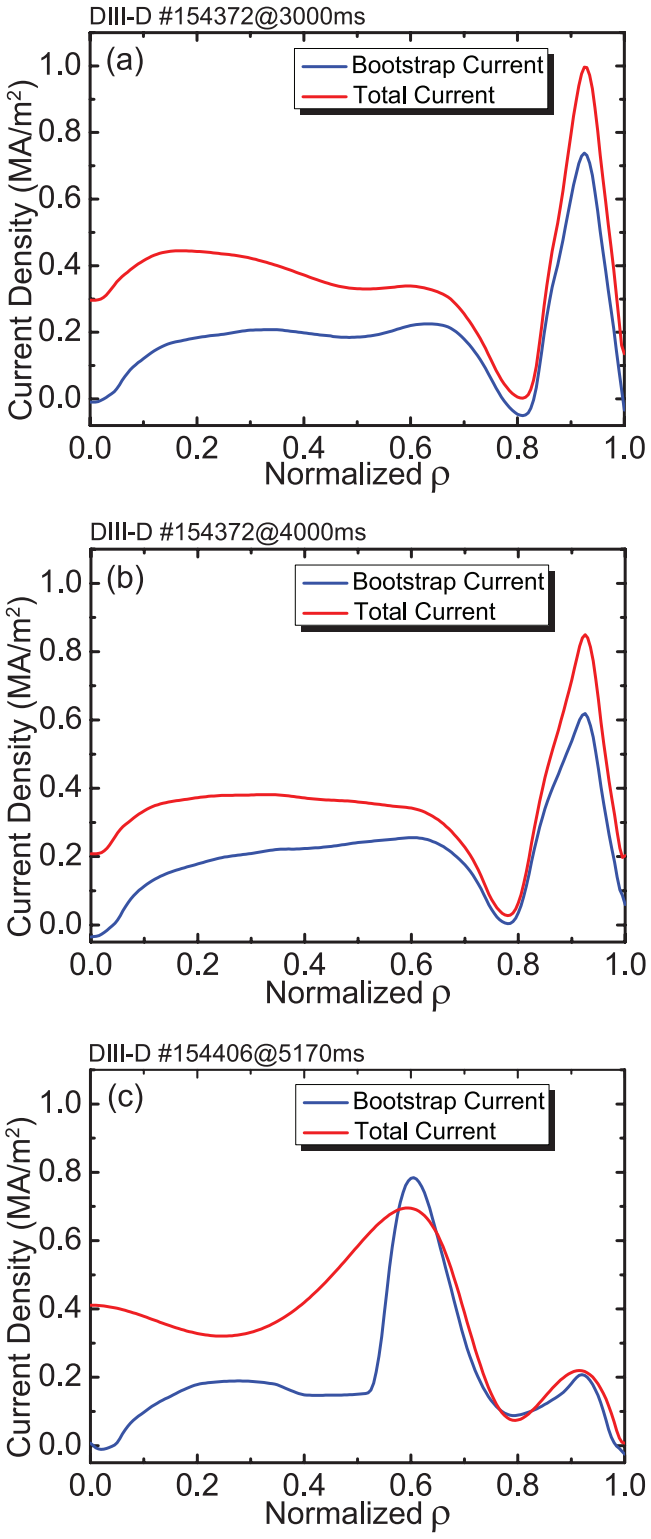

Figure 4. Total and bootstrap current density profiles for the DIII-D high-β_P discharge 154372 at $t = 3.0$ s, 4.0 s and discharge 154406 at $t = 5.17$ s. The bootstrap current is calculated by NEO.

the $E \times B$ flow shear has negligible effect on the ion turbulent energy transport in discharge 154406 at $t = 5.17$ s as shown in figure 6(*f*). The experimental ion temperature profiles for these high-β_P discharges can be well predicted with only the NEO neoclassical transport model as shown in figure 7. The ion energy transport in the DIII-D high-β_P discharge 154366

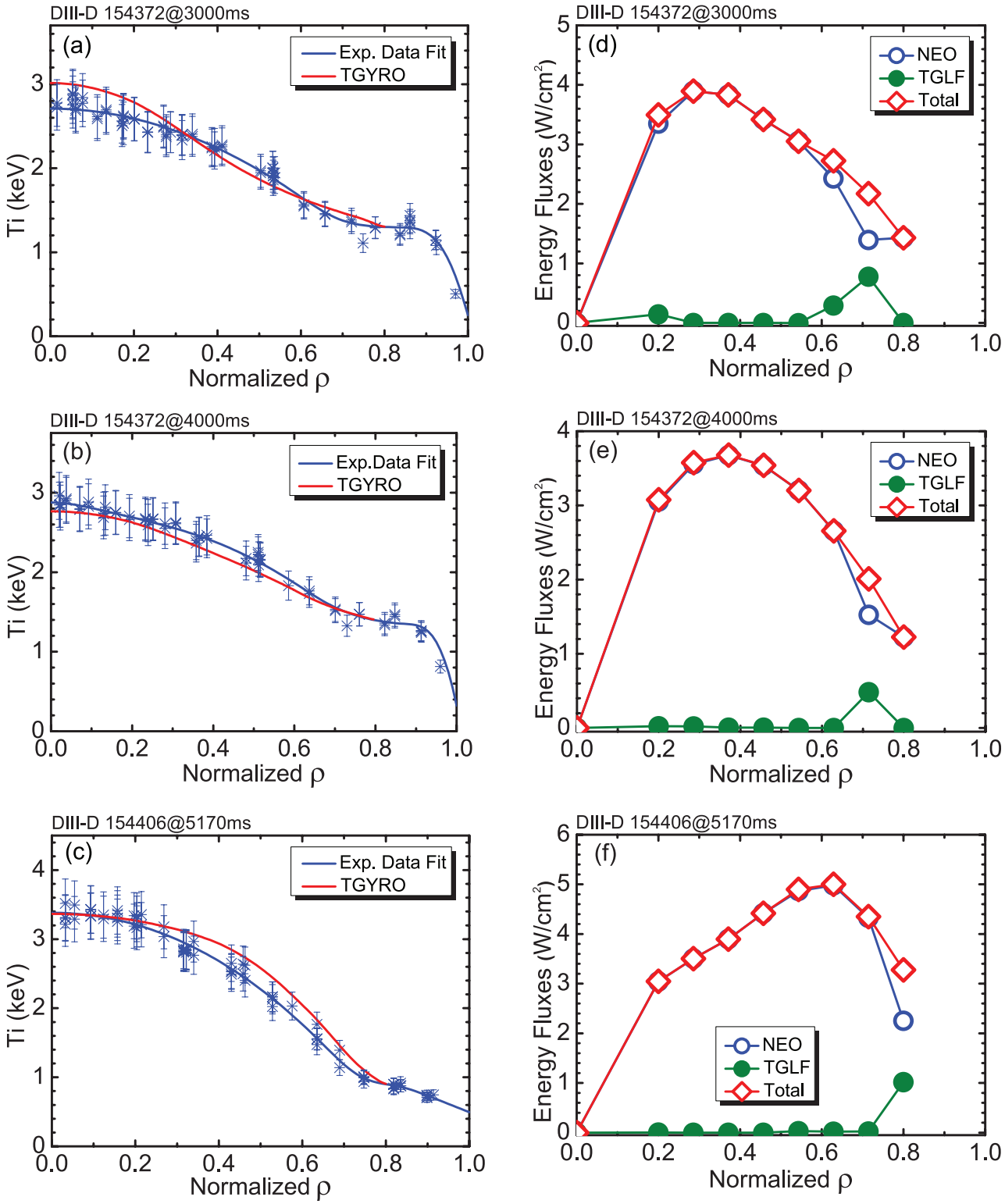

Figure 5. (*a*)–(*c*) Ion temperature profiles from the experimental data fit (blue line) and the TGYRO predictions (red) for the DIII-D high-β_P discharge 154372 at $t = 3.0$ s, 4.0 s and discharge 154406 at $t = 5.17$ s; (*d*)–(*f*) profiles of the total ion energy flux (red), the ion neoclassical energy flux (blue) and the ion turbulent energy flux (olive) calculated with NEO and TGLF respectively. The electron temperature profile and other profiles are kept fixed in the simulations.

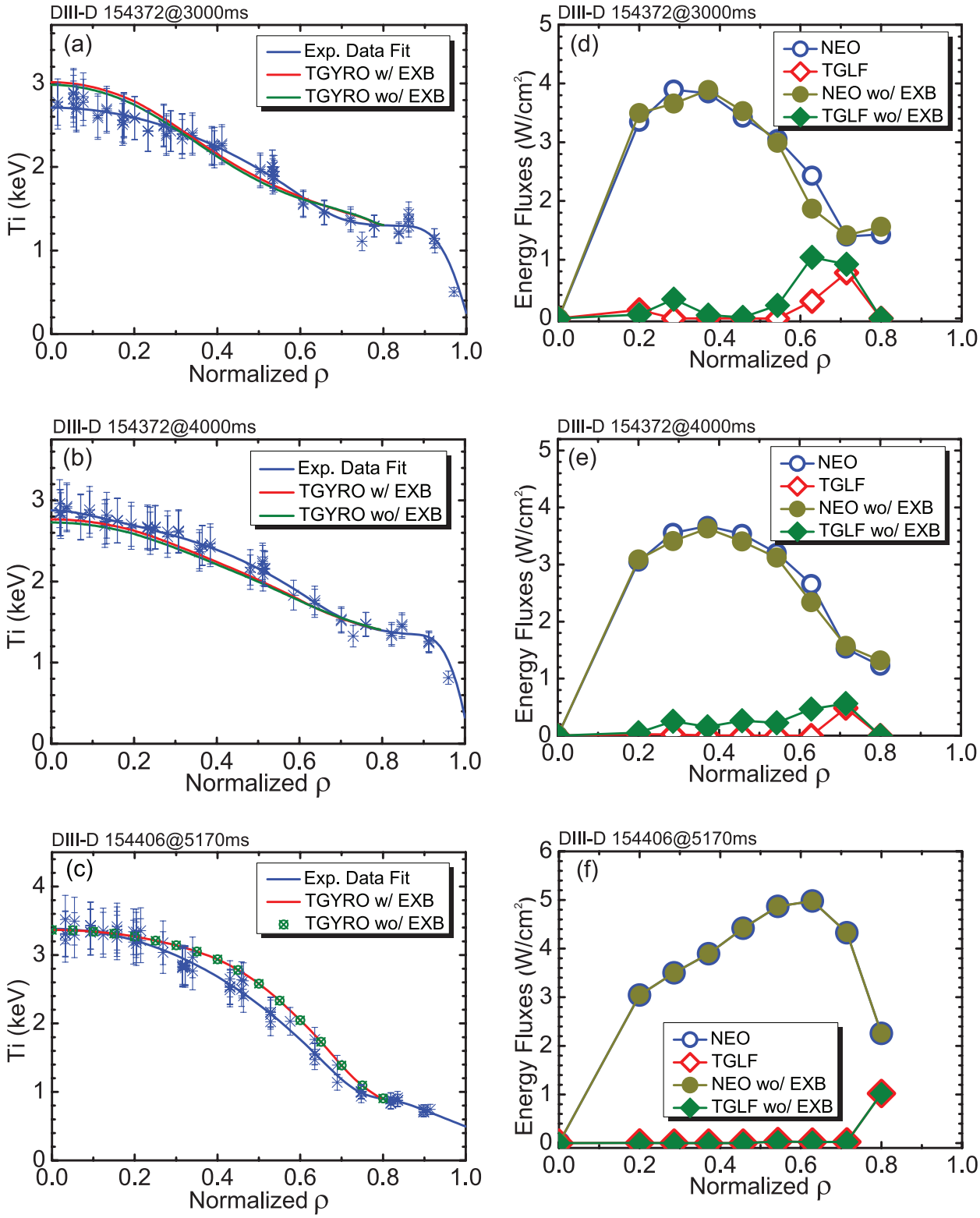

Figure 6. (*a*)–(*c*) Ion temperature profiles from the experimental data fit (blue) and the TGYRO predictions with (red) and without $E \times B$ (olive) flow shear for the DIII-D high-β_P discharge 154372 at $t = 3.0$ s, 4.0 s and discharge 154406 at $t = 5.17$ s; (*d*)–(*f*) profiles of the calculated ion turbulent energy flux and neoclassical energy flux with and without $E \times B$ flow shear.

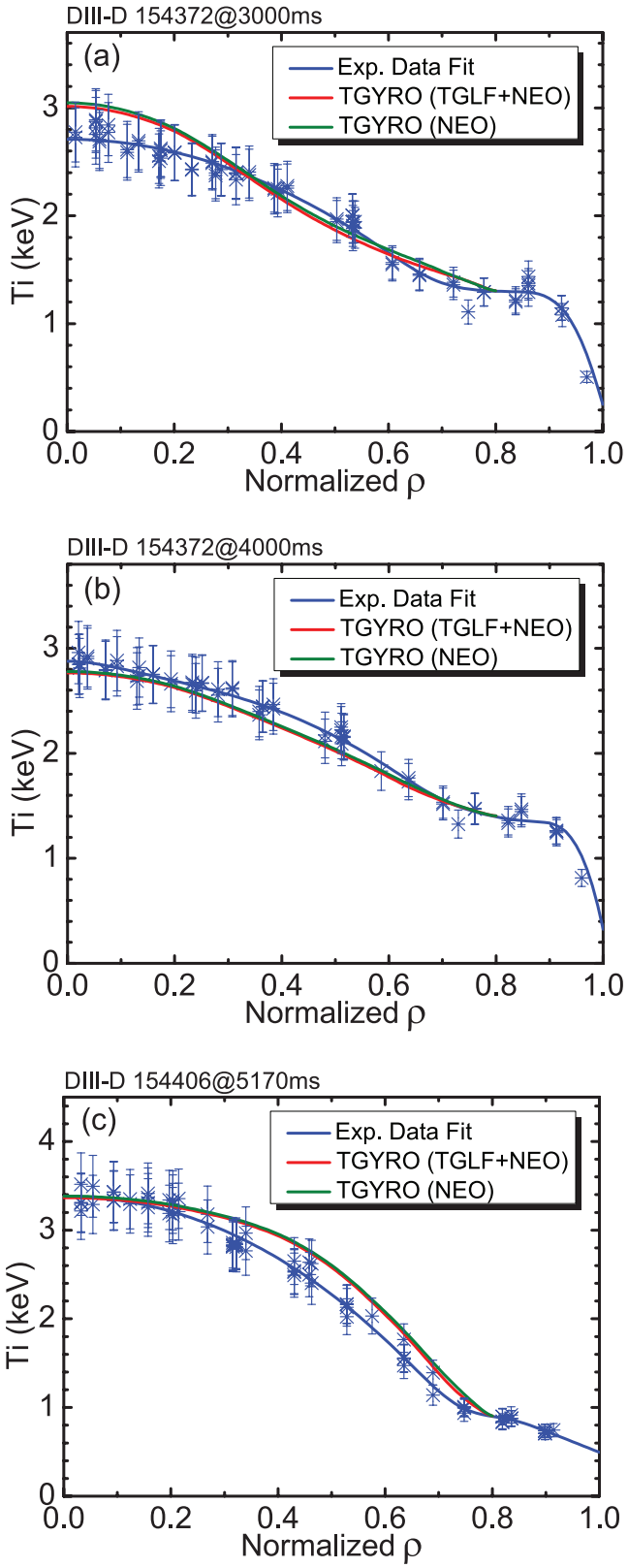

Figure 7. (*a*)–(*c*) Ion temperature profiles from the experimental data fit (blue line) and the TGYRO predictions with TGLF + NEO (red) and only with NEO (olive) for the DIII-D high-β_P discharge 154372 at $t = 3.0$ s, 4.0 s and discharge 154406 at $t = 5.17$ s respectively. The electron temperature profile and other profiles are kept fixed in the simulations.

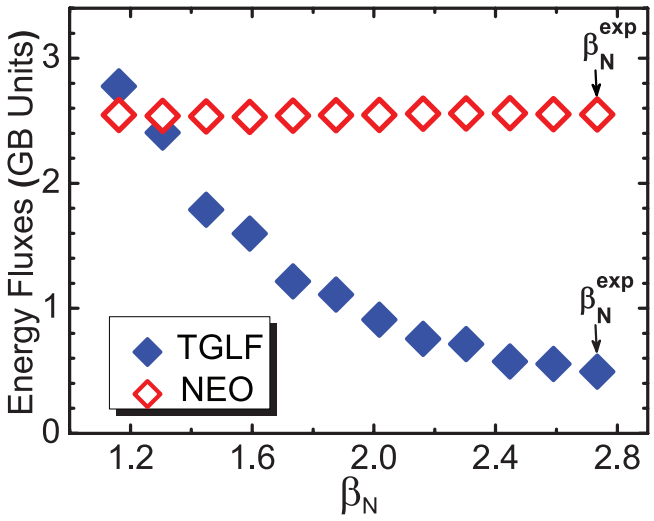

Figure 8. Ion turbulent and neoclassical energy fluxes calculated with TGLF and NEO versus β_N. The label points shows the calculated ion turbulent and neoclassical energy fluxes with the experimental β_N (discharge 154372 at $t = 4.0$ s and $\rho = 0.63$).

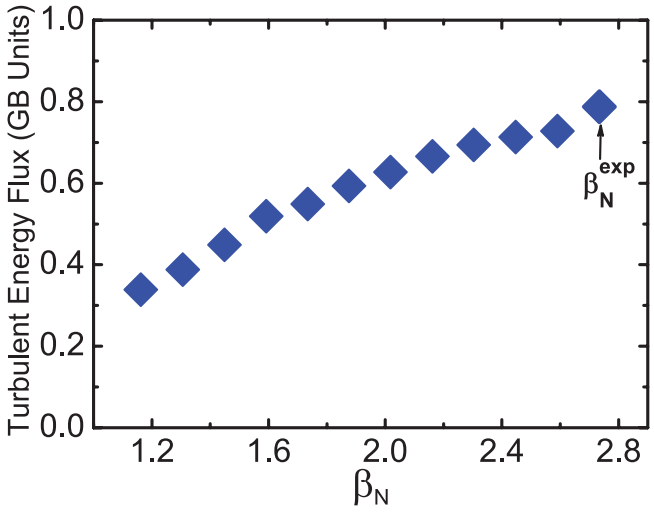

Figure 9. Ion turbulent energy fluxes calculated with TGLF versus β_N. The label point shows the calculated ion turbulent energy flux with the experimental β_N (discharge 154372 at $t = 4.0$ s and $\rho = 0.71$).

also has this characteristic [8]. These TGLF + NEO simulation results are consistent with the experimental measurements that there is no significant change in measured fluctuations in these high-β_P discharges with lower and higher plasma rotation and with the gyrokinetic simulations [37].

The Shafranov shift, which increases with the pressure gradient and β_P or β_N increased, also has a stabilizing effect on the transport in the tokamak plasmas [38]. The Shafranov shift cannot be neglected in the high-β_P discharges. To investigate whether the Shafranov shift plays a role in the suppression of the ion turbulent energy transport in the high-β_P discharges, the ion turbulent energy fluxes will be calculated by TGLF for a sequence of model equilibria, which are generated by scaling down the pressure profile used in the EFIT

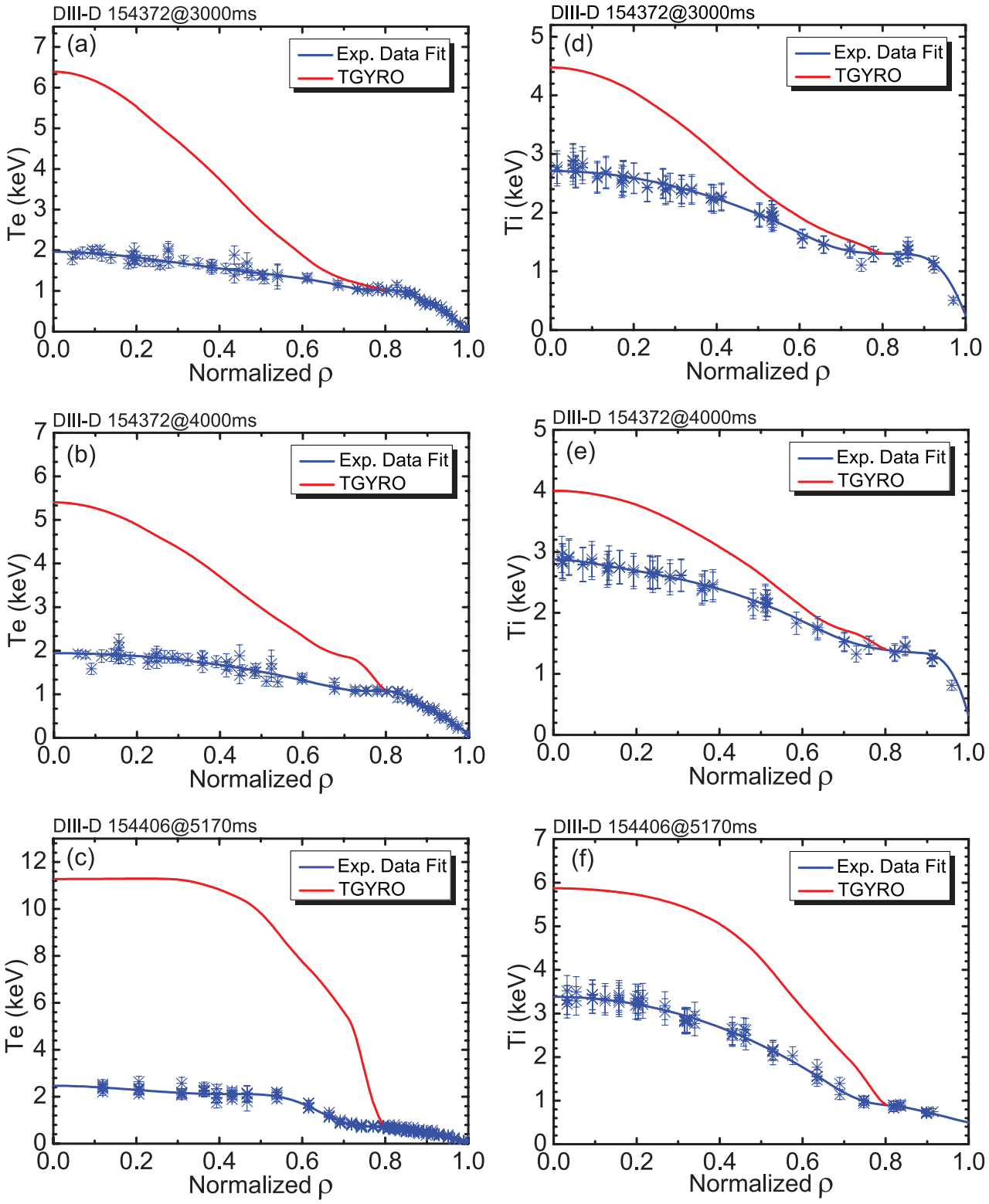

Figure 10. (*a*)–(*c*) Electron and (*d*)–(*f*) ion temperature profiles from the experimental data fit (blue) and the TGYRO predictions (red) for the DIII-D high-β_P discharge 154372 at $t = 3.0$ s, 4.0 s and discharge 154406 at $t = 5.17$ s. The electron turbulent energy flux is calculated with TGLF.

[39] equilibrium calculation while holding the plasma gradients and the q profile nearly fixed. Then the β_N scanning for the ion turbulent energy fluxes is done with the plasma profiles fixed, which are taken from the DIII-D high-β_P discharge 154372 at $t = 4.0$ s. The impact of the Shafranov shift or β_N on the ion turbulent energy transport could be studied through this method.

The ion turbulent energy fluxes calculated by TGLF at $\rho = 0.63$, which is in the ion-ITB region, decrease with β_N increased as shown in figure 8. Hence, the Shafranov shift has

a stabilizing effect on the ion turbulent energy transport in this region. The ion neoclassical energy fluxes calculated by NEO are also shown in figure 8, which are not sensitive to β_N. The ion energy transport is dominated by the neoclassical energy transport with the larger β_N. The ion turbulent energy flux is comparable with or even larger than the ion neoclassical energy flux with β_N decreased to ~1.25. This indicates that the Shafranov shift could play a role in the formation of ion-ITB due to the suppression of the ion turbulent transport below the neoclassical level. In the ion-ITB foot, at $\rho = 0.71$, the ion turbulent energy fluxes calculated by TGLF increase with β_N increased as shown clearly in figure 9. These calculations are consistent with the shape of the experimental ion temperature profile as shown in figure 2(*b*). The destabilization effect of the Shafranov shift in the ion-ITB foot makes the ion temperature profile flatter there, while the steeper ion temperature profile in the ion-ITB region is due to the stabilization effect of the Shafranov shift.

3.2. Electron energy transport under-predicted with TGLF

In these series of simulations, both the ion and electron temperature profiles are predicted by TGYRO with the boundary condition at $\rho = 0.8$ for the DIII-D high-β_P discharge 154372 at $t = 3.0$ s, 4.0 s and discharge 154406 at $t = 5.17$ s as shown in figure 10(*a*)–(*f*). The electron turbulent energy flux is calculated by TGLF with the default ETG turbulence saturation level. Both the predicted ion and electron temperature as shown by the red lines are much higher than the experimental measured values as shown by the blue lines. The higher predicted ion temperature, which is not as shown in figures 5(*a*)–(*c*), is due to the dynamic ion-electron energy exchange. The main reason for the increased ion temperature is that the electron energy transport is dramatically under-predicted by TGLF. There is a significant shortfall in the electron energy transport over the whole core plasma with the TGLF predictions. The electron particle transport in these high-β_P discharges is also under-predicted by TGLF when only the electron density profiles are predicted with TGYRO as shown in figures 11(*a*)–(*c*). The near edge transport shortfall has been found in DIII-D L-mode plasmas [40–45] and Alcator C-Mod L-mode plasmas [46] but such a large shortfall over most of the core is unprecedented.

An increase in the ion-scale turbulent transport is ruled out by the lack of measurable ion-scale turbulence in these high-β_P discharges. Recent multi-scale simulations have shown that there is strong coupling between the ion and electron scales in the streamer regime characterized by the high electron-scale turbulence; the contribution of the electron-scale (high-k) turbulence increases when the drive for the ion-scale turbulence is weak [47–50]. The TGLF saturation model for the high-k ETG modes is based on a single multi-scale GYRO simulation that included both ion and electron scales [51]. There is a $1/k_y^{C_3}$ (k_y is the normalized poloidal wave number) factor within the saturation rule for the nonlinear intensity of the turbulence due to each high-k ETG mode ($k_y > 1$). By default $C_3 = 1.25$ is used which yields the GYRO simulation predicted a ratio of $\chi_{\text{high-}k}/\chi_{\text{e,low-}k}$

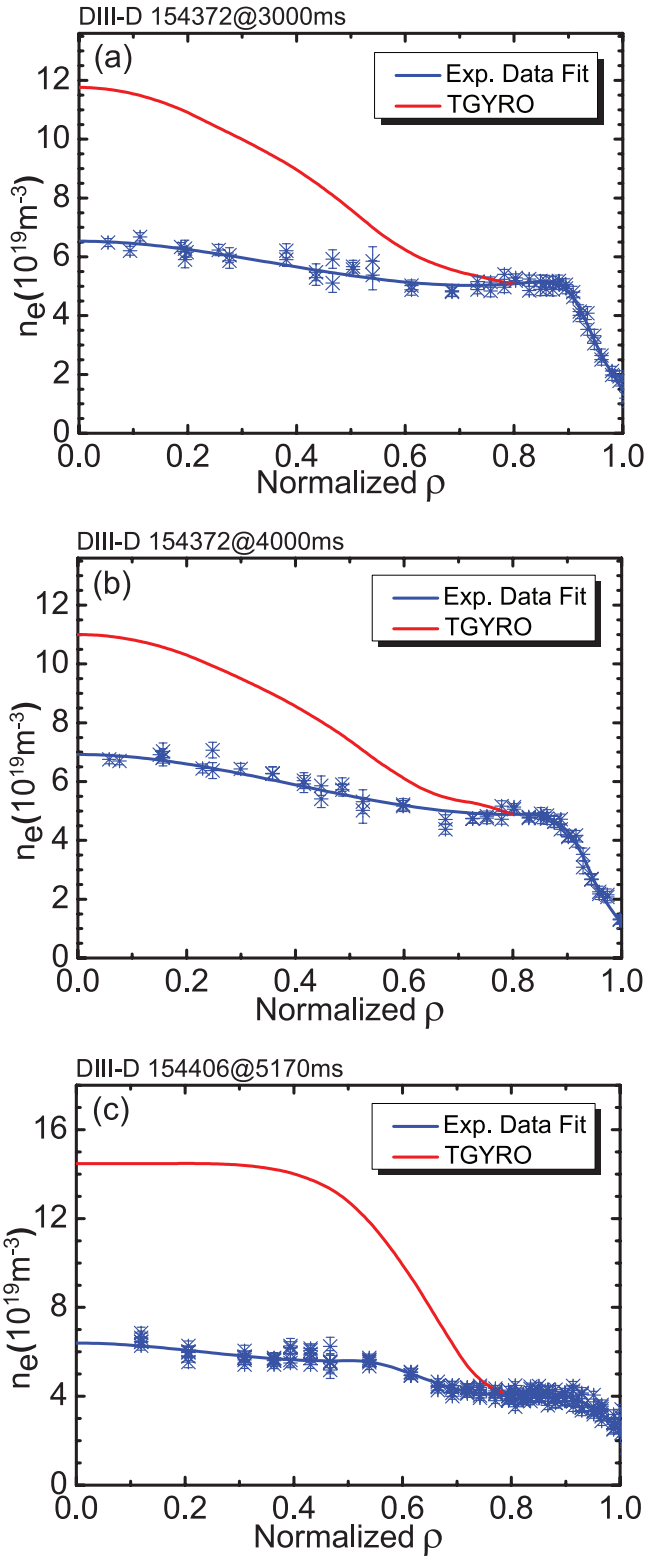

Figure 11. Electron density profiles from the experimental data fit (blue) and the TGYRO predictions (red) for the DIII-D high-β_P (*a*) and (*b*) discharge 154372 at $t = 3.0$ s, $t = 4.0$ s, and (*c*) discharge 154406 at $t = 5.17$ s. The other profiles are kept fixed in the simulations.

of approximately 12% for the GA standard case [17, 18]. The transport level for the ETG modes turbulence increases with the factor $1/k_y^{C_3}$ increased. To investigate the possibility that ETG instabilities could cause the electron energy transport in these

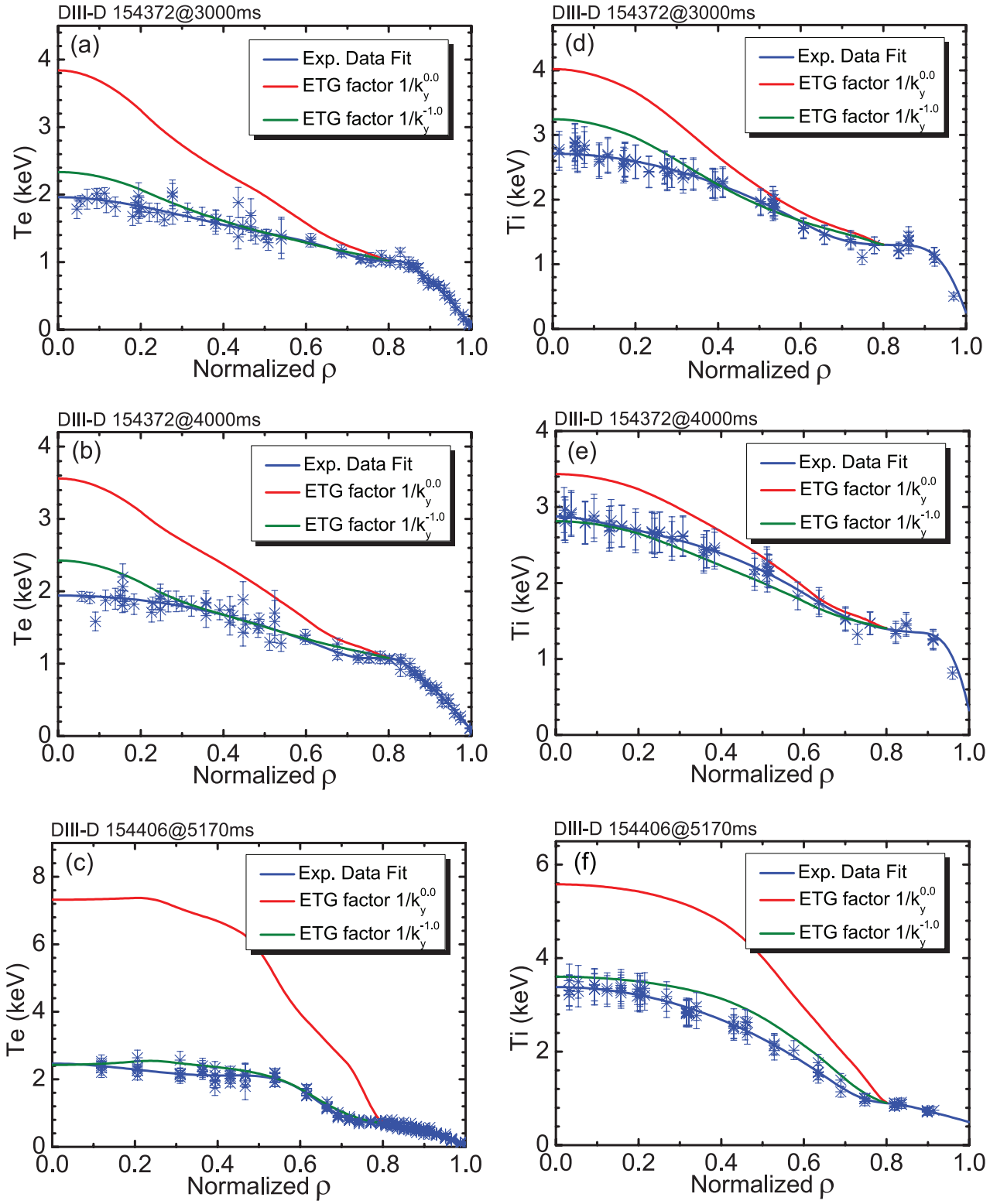

Figure 12. (*a*)–(*c*) Electron and (*d*)–(*f*) ion temperature profiles from the experimental data fit (blue) and the TGYRO predictions with the ETG turbulence saturation amplitude multiplied by $k_y^{1.25}$ (red) and $k_y^{2.25}$ (olive) respectively for $k_y > 1$ compared to the standard setting in TGLF for the DIII-D high-β_P discharge 154372 at $t = 3.0$ s, 4.0 s and discharge 154406 at $t = 5.17$ s.

high-β_P discharges, the saturated turbulence level for the high-k ETG modes used in TGLF is increased artificially. By increasing the saturated turbulence level for the ETG modes, the predicted ion and electron temperature profiles can well match the experimental measured ion and electron temperature profiles as shown in figures 12(*a*)–(*f*). TGLF can predict the experimental electron temperature profiles with the ETG turbulence saturated amplitude multiplied by a factor $k_y^{2.25}$ compared to the standard setting as shown by the olive lines. The enhanced ETG turbulence transport due to the strong coupling of the high-k modes

to the low-k modes could play an important role for the electron energy transport in these high-β_P discharges [47–50]. Multi-scale non-linear simulations need to be done for these high-β_P discharges in order to validate this conjecture.

4. Summary and conclusions

The energy transport analyses of the DIII-D high-β_P EAST-demonstration discharges have been performed using TGYRO transport package with the TGLF turbulent and NEO neoclassical transport models. The results show that in these high-β_P discharges the ion energy transport is very much neoclassical and the ion temperature profiles predicted by TGYRO agree closely with the experimental measured profiles. The ion energy transport is largely insensitive to reductions in the $E \times B$ flow shear. The ion energy transport is still dominated by the neoclassical contribution even without the $E \times B$ flow shear stabilization effect. The Shafranov shift plays a role in the suppression of the ion turbulent energy transport and the formation of ion-ITB. A significant shortfall in the electron energy transport over the whole core plasma is found with TGLF predictions for these high-β_P discharges. TGYRO can successfully predict the experimental ion and electron temperature profiles by artificially increasing the saturated turbulence level for ETG driven modes computed in TGLF. This indicates a possible resolution to the shortfall in the predicted transport.

Acknowledgments

This work was supported by US DOE under DE-FC02-04ER54698 and DE-FG03-95ER54309, the National Natural Science Foundation of China under Grant Nos. 11575246, 11105182, 11422546, 11575235 and the National Magnetic Confinement Fusion Program of China under Contract No. 2014GB106001, 2015GB101000, No. 2015GB102001 and No. 2015GB110001.

References

[1] Bickerton R.J., Connor J.W. and Taylor J.B. 1971 *Nat. Phys. Sci.* **229** 110
[2] Rosenbluth M.N., Hazeltine R.D. and Hinton F.L. 1972 *Phys. Fluids* **15** 116
[3] Hinton F.L. and Hazeltine R.D. 1976 *Rev. Mod. Phys.* **48** 239
[4] Zarnstorff M.C. *et al* 1988 *Phys. Rev. Lett* **60** 1306
[5] Politzer P.A. *et al* 2005 *Nucl. Fusion* **45** 417
[6] Wan B. *et al* 2014 *Proc. of 41st EPS Conf. on Plasma Physics (Berlin, Germany, 23–27 June 2014)* vol 38F (http://ocs.ciemat.es/EPS2014PAP/pdf/O2.104.pdf)
[7] Gong X. *et al* 2014 Development of fully noninductive scenario at high bootstrap current fraction for steady state tokamak operation on DIII-D and EAST *25th IAEA Fusion Energy Conf.* EX/P2-39 *(St Petersburg, Russian Federation, 13–18 October 2014)* (www.fec2014.org/en)
[8] Garofalo A. *et al* 2015 *Nucl. Fusion* **55** 123025
[9] Ren Q. *et al* 2016 *Phys. Plasmas* **23** 062511
[10] Ding S. *et al* 2017 *Nucl. Fusion* **57** 022016
[11] Wan B. *et al* 2015 *Nucl. Fusion* **55** 104015
[12] Staebler G.M., Kinsey J.E. and Waltz R.E. 2005 *Phys. Plasmas* **12** 102508
[13] Staebler G.M., Kinsey J.E. and Waltz R.E. 2007 *Phys. Plasmas* **14** 055909
[14] Staebler G.M. *et al* 2013 *Phys. Rev. Lett.* **110** 055003
[15] Staebler G.M. 2013 *Nucl. Fusion* **53** 113017
[16] Candy J. and Waltz R.E. 2003 *J. Comput. Phys.* **186** 545
[17] Kinsey J.E., Staebler G.M. and Waltz R.E. 2008 *Phys. Plasmas* **15** 055908
[18] Kinsey J.E. *et al* 2010 *Phys. Plasmas* **17** 122315
[19] Kinsey J.E. *et al* 2015 *Phys. Plasmas* **22** 012507
[20] Schmitz L. *et al* 2008 *Phys. Rev. Lett.* **100** 035002
[21] Mantica P. *et al* 2011 *Phys. Rev. Lett.* **107** 135004
[22] Porkolab M. *et al* 2012 *Plasma Phys. Control. Fusion* **54** 124029
[23] Sommer F. *et al* 2015 *Nucl. Fusion* **55** 033006
[24] Beli E.A. and Candy J. 2008 *Plasma Phys. Control. Fusion* **50** 095010
[25] Beli E. and Candy J. 2009 *Plasma Phys. Control. Fusion* **51** 075018
[26] Beli E. and Candy J. 2012 *Plasma Phys. Control. Fusion* **54** 015015
[27] Ren Q. *et al* 2015 *Plasma Phys. Control. Fusion* **57** 025020
[28] Staebler G.M. *et al* 2014 *Phys. Plasmas* **21** 055902
[29] Candy J. *et al* 2009 *Phys. Plasmas* **16** 060704
[30] Candy J. 2013 *Phys. Plasmas* **20** 082503
[31] Meneghini O. and Lao L.L. 2013 *Plasma Fusion Res.* **8** 2403009
[32] Meneghini O. *et al* 2015 *Nucl. Fusion* **55** 083008
[33] Pfeiffer W.W., Davidson R.H., Miller R.L. and Waltz R.E. 1980 ONETWO: a computer code for modeling plasma transport in tokamaks *General Atomics Report GA-A16178* (http://fusion.gat.com/THEORY/onetwo)
[34] Burrell K.H. 1997 *Phys. Plasmas* **4** 1499
[35] Terry P.W. 2000 *Rev. Mod. Phys.* **72** 109
[36] Stallard B.W. *et al* 1999 *Phys. Plasmas* **6** 1978
[37] Pan C. *et al* 2016 Energy transport analyses of DIII-D high-β_P EAST-Demonstration discharges *US Transport Task Force Workshop (Denver, USA, 29 March–1 April, 2016)* (www-internal.psfc.mit.edu/TTF2016/agenda.html)
[38] Beer M.A. *et al* 1997 *Phys. Plasmas* **4** 1792
[39] Lao L.L. *et al* 1985 *Nucl. Fusion* **25** 1421
[40] Rhodes T.L. *et al* 2011 *Nucl. Fusion* **51** 063022
[41] White A.E. *et al* 2008 *Phys. Plasmas* **15** 056116
[42] White A.E. *et al* 2010 *Phys. Plasmas* **17** 056103
[43] Holland C. *et al* 2009 *Phys. Plasmas* **16** 052301
[44] Holland C. *et al* 2011 *Phys. Plasmas* **18** 056113
[45] DeBoo J.C. *et al* 2010 *Phys. Plasmas* **17** 056105
[46] Howard N.T. *et al* 2013 *Phys. Plasmas* **20** 032510
[47] Howard N.T., Holland C., White A.E., Greenwald M. and Candy J. 2016 *Nucl. Fuion* **56** 014004
[48] Staebler G.M. and Candy J. 2015 The impact of zonal flows on the performance predictions for ITER *57th Annual Meeting of the APS Division of Plasma Physics (Savannah, USA, 16–20 November, 2015)* (http://meeting.aps.org/Meeting/DPP15/Session/TO6.14)
[49] Staebler G.M., Howard N., Candy J. and Holland C. 2016 A model for the saturation of multi-scale turbulence *US Transport Task Force Workshop (Denver, USA, 29 March–1 April, 2016)* (www-internal.psfc.mit.edu/TTF2016/agenda.html)
[50] Staebler G.M., Howard N.T., Candy J. and Holland C. 2016 A model of saturation of coupled electron and ion scale gyrokinetic turbulence *26th IAEA Fusion Energy Conf.* TH/P2-8 *(Kyoto, Japan, 17–22 October, 2016)* (www.fec2016.jp)
[51] Candy J., Waltz R.E. and Fehey M.R. 2007 *J. Phys.:Conf. Ser.* **78** 012008